The Application of the Point Matching Method to the Analysis of Microstrip Lines with Finite Metallization Thickness

STEFAN KOSSLOWSKI, MEMBER, IEEE, FRANK BÖGELSACK, MEMBER, IEEE, AND INGO WOLFF, FELLOW, IEEE

Abstract — **This paper presents an attempt to calculate the characteristics of a shielded microstrip line with finite metallization thickness by the point matching method (PMM). Numerical results are presented in order to assert the validity of this approach in cases of large values of strip width to thickness ratio. It is found that an increase in the strip thickness is always associated with difficulties in convergence. This can be easily recognized if the field distribution is taken into account.**

I. Introduction

THE MODE MATCHING technique (MMT) is usually used in the analysis of shielded microstrip lines with finite metallization thickness. A basic disadvantage of this method is that 90° edges of the strip metallization cannot be avoided (in theory) when calculating the unknown field expansion coefficients. In most cases 90° edges cause difficulties in the convergence of the characteristic impedance and the effective dielectric constant.

In this paper, an attempt is made to solve these problems using the point matching method (PMM). The advantage in this case is that the method does not depend on a special geometry of the strip metallization. Therefore, the microstrip line can be described by structures as shown in Fig. 1. Some interesting papers have been published dealing with the solution of field problems in hollow-piped waveguides of arbitrary geometry by using the PMM (for example [2]–[4]). Thus it is expected that an application of this method to microstrip lines is possible if some restricting conditions pointed out in [5]–[7] are taken into account.

II. Theoretical Approach

The symmetry of the considered waveguide allows the description of the electromagnetic field as a superposition of even and odd modes. In both cases the procedure for using the PMM is identical. Hence it is sufficient to investigate one mode only (e.g. the quasi-TEM mode, the first even mode) in order to study the characteristics of this approach.

To calculate the electromagnetic field distribution, the stripline is subdivided into two areas as shown in Fig. 2.

Manuscript received October 15, 1987; revised February 29, 1988.

The authors are with the Department of Electrical Engineering and Sonderforschungsbereich 254, Duisburg University, D-4100 Duisburg, West Germany.

IEEE Log Number 8821759.

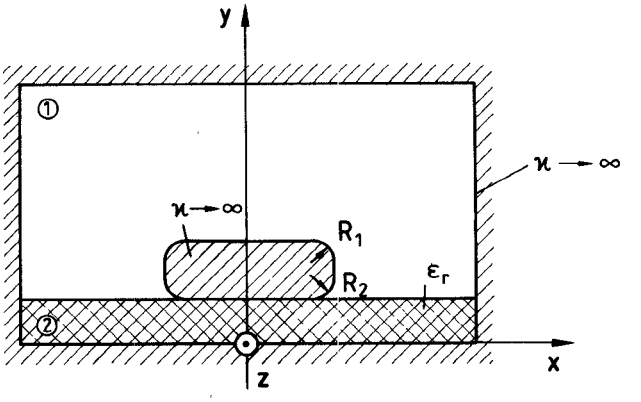

Fig. 1. Description of the microstrip line that is to be calculated by the PMM. Area 1: $\epsilon^{(1)} = \epsilon_0$; $\mu^{(1)} = \mu_0$ (air-filled region). Area 2: $\epsilon^{(2)} = \epsilon_r \cdot \epsilon_0$; $\mu^{(2)} = \mu_0$ (dielectric region).

The field components within each of these areas are described by an electric and a magnetic vector potential with a component in the z direction (coordinate of wave propagation):

$$\vec{A} = \Psi^E \cdot \vec{u}_z \quad \text{and} \quad \vec{F} = \Psi^H \cdot \vec{u}_z \tag{1}$$

with $\vec{u}_z$ the unit vector in the z direction.

This leads to the following potential functions:

Area 1:

$$\Psi_1^E = \sum_{n=1}^{\infty} A_n \cdot \cos\left(k_x^{(1)}(n) \cdot x\right) \cdot \sin\left(k_y^{(1)}(n) \cdot (y-c)\right) \cdot e^{-jk_z \cdot z}$$

$$\Psi_1^H = \sum_{n=1}^{\infty} B_n \cdot \sin\left(k_x^{(1)}(n) \cdot x\right) \cdot \cos\left(k_y^{(1)}(n) \cdot (y-c)\right) \cdot e^{-jk_z \cdot z} \tag{2}$$

Area 2:

$$\Psi_2^E = \sum_{n=1}^{\infty} C_n \cdot \cos\left(k_x^{(2)}(n) \cdot x\right) \cdot \sin\left(k_y^{(2)}(n) \cdot y\right) \cdot e^{-jk_z \cdot z}$$

$$\Psi_2^H = \sum_{n=1}^{\infty} D_n \cdot \sin\left(k_x^{(2)}(n) \cdot x\right) \cdot \cos\left(k_y^{(2)}(n) \cdot y\right) \cdot e^{-jk_z \cdot z}.$$

For the numerical analysis the series have to be truncated at a truncation index N. For the microstrip line shown in

0018-9480/88/0800-1265$01.00 ©1988 IEEE

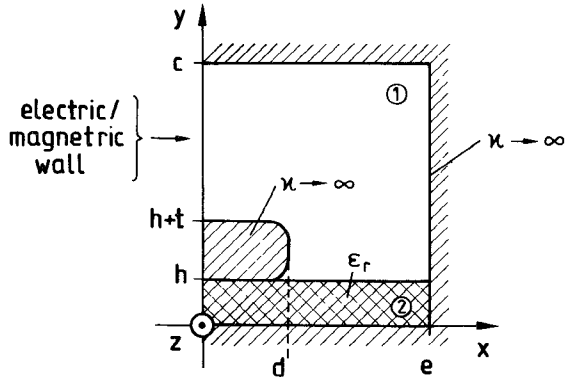

Fig. 2. Subdividing the waveguide in order to make use of its symmetry. Region 1: air-filled region. Region 2: dielectric region.

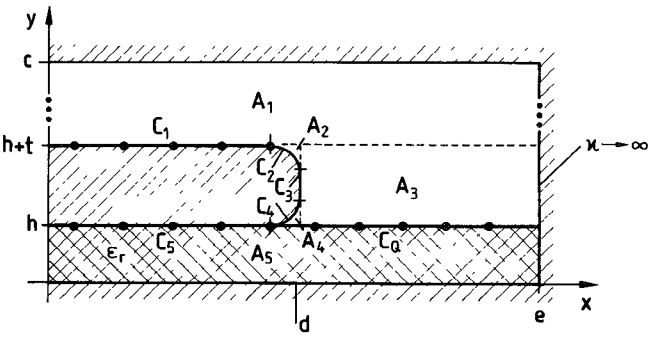

Fig. 3. Defined curves $\mathbb{C}_\nu$ ($\nu=1,2,3,4,5$) and $\mathbb{C}_Q$ describing the metallization and the air–dielectric interface as well as the matching points and the subareas $\mathbb{A}_\mu$ ($\mu=1,2,3,4,5$).

Fig. 2 the relationship between the appearing eigenvalues is given by

$$k_x^{(1),(2)}(n)=\left(n-\frac{1}{2}\right)\cdot\frac{\pi}{e}$$

$$k_y^{(1)}(n)=\sqrt{k_0^2-k_z^2-k_x^{(1)^2}(n)}$$

$$k_y^{(2)}(n)=\sqrt{\epsilon_r k_0^2-k_z^2-k_x^{(2)^2}(n)} \tag{3}$$

and according to [1] the electromagnetic field is obtained from the potentials by

$$E_x=\frac{1}{j\omega\epsilon}\cdot\frac{\partial^2\Psi^E}{\partial x\,\partial z}-\frac{\partial\Psi^H}{\partial y}$$

$$E_y=\frac{1}{j\omega\epsilon}\cdot\frac{\partial^2\Psi^E}{\partial y\,\partial z}+\frac{\partial\Psi^H}{\partial x}$$

$$E_z=\frac{1}{j\omega\epsilon}\cdot\left(\frac{\partial^2}{\partial z^2}+k^2\right)\Psi^E$$

$$H_x=\frac{\partial\Psi^E}{\partial y}+\frac{1}{j\omega\mu}\cdot\frac{\partial^2\Psi^H}{\partial x\,\partial z}$$

$$H_y=-\frac{\partial\Psi^E}{\partial x}+\frac{1}{j\omega\mu}\cdot\frac{\partial^2\Psi^H}{\partial y\,\partial z}$$

$$H_z=\frac{1}{j\omega\mu}\cdot\left(\frac{\partial^2}{\partial z^2}+k^2\right)\Psi^H. \tag{4}$$

The description of the electromagnetic field by the series of eigenfunctions as described above ensures that the wave equation and the boundary conditions at the conducting shielding are fulfilled.

To satisfy the continuity conditions for the electromagnetic field at the interface between the two regions (Fig. 2) as well as on the strip metallization, three different procedures based on the PMM will be presented. Therefore, in a cross section such that $z=\text{const.}$ the waveguide is described by curves $\mathbb{C}_1\cdots\mathbb{C}_5$ (metallization) and $\mathbb{C}_Q$ (dielectric–air interface) (Fig. 3). On each of the curves $\mathbb{C}_\nu$ ($\nu=1,2,3,4,5$) P_ν fixed points $S_\nu(i)$, with $i=1,2,\cdots,P_\nu$, are determined. On $\mathbb{C}_Q$ there are chosen Q points with the coordinates $(x_Q(i)|y_Q(i))$, $(i=1,2,\cdots,Q)$.

The first approach is based on the requirement that the boundary conditions at the test points $S_1(i)\cdots S_5(i)$ described by the coordinates $(x_\nu(i)|y_\nu(i))$ be satisfied by the vector potentials so that

$$\Psi^E\Big|_{\substack{x=x_\nu(i)\\ y=y_\nu(i)}}=0 \tag{5}$$

as well as

$$\frac{\partial\Psi^H}{\partial\vec{n}}\Big|_{\substack{x=x_\nu(i)\\ y=y_\nu(i)}}=0. \tag{6}$$

At the dielectric–air interface the continuity conditions have to be satisfied by the tangential electromagnetic field components:

$$E_{\tan}^{(1)}\Big|_{\substack{x=x_Q(i)\\ y=y_Q(i)}}=E_{\tan}^{(2)}\Big|_{\substack{x=x_Q(i)\\ y=y_Q(i)}},\qquad i=1\cdots Q \tag{7}$$

and

$$H_{\tan}^{(1)}\Big|_{\substack{x=x_Q(i)\\ y=y_Q(i)}}=H_{\tan}^{(2)}\Big|_{\substack{x=x_Q(i)\\ y=y_Q(i)}},\qquad i=1\cdots Q. \tag{8}$$

If all boundary and continuity equations are formulated, a system of $2\cdot\sum_{\nu=1}^{5}P_\nu+4\cdot Q$ equations is derived which can be expressed in matrix form as follows:

$$\vec{\vec{M}}\cdot\vec{K}=\vec{0}. \tag{9}$$

$\vec{K}$ is the coefficient vector described by

$$\vec{K}=(A_1,\cdots,A_N,B_1,\cdots,B_N,C_1,\cdots,C_N,D_1,\cdots,D_N)^T. \tag{10}$$

The system matrix $\vec{\vec{M}}$ exists of $2\cdot\sum_{\nu=1}^{5}P_\nu+4\cdot Q$ rows and $4\cdot N$ columns.

A nontrivial solution of the above set of homogeneous equations is obtained if and only if

$$\det\vec{\vec{M}}=0. \tag{11}$$

Hence, in this approach, the relationship between the number of test points on the one hand and the truncation index N on the other hand is given by

$$2\cdot\sum_{\nu=1}^{5}P_\nu+4\cdot Q=4\cdot N. \tag{12}$$

If this condition is satisfied, the eigenvalue problem, e.g. of

determining the effective dielectric constant ϵ_{eff}, can be solved.

There are possibilities other than the one shown above which take the continuity conditions into account. A second solution (method 2) can be obtained if the boundary conditions on the strip metallization are satisfied by the field components instead of the vector potentials (method 1). Because only a finite number N of eigenfunctions is used, these formulations are not equivalent. Using this method, the rank of the system matrix $\overleftrightarrow{M}$ and the correlation between the number of test points and the number of eigenfunctions is the same as that given in (12).

A third method to solve the problem is to combine the PMM and the MMT. This means that the continuity conditions for the electric fields on the curves $\mathbb{C}_5$ and $\mathbb{C}_Q$ (Fig. 3) are fulfilled by using the orthogonality of the eigenfunctions in the interval $[0|e]$. Therefore the tangential components of the electric fields are tested by

$$\int_{d-R_2}^{e}\left\{E_x^{(1)}|_{y=h}\cdot\Phi_{an}(x)\right\}dx=\int_0^e\left\{E_x^{(2)}|_{y=h}\cdot\Phi_{an}(x)\right\}dx$$

$$\int_{d-R_2}^{e}\left\{E_z^{(1)}|_{y=h}\cdot\Phi_{bn}(x)\right\}dx=\int_0^e\left\{E_z^{(2)}|_{y=h}\cdot\Phi_{bn}(x)\right\}dx. \tag{13}$$

Testing with the eigenfunctions of the potential functions instead of the arbitrary functions Φ_{an} and Φ_{bn} delivers expressions for the unknown coefficients C_ν and D_ν in the form of series that depend only on A_ν and B_ν.

The boundary conditions for the electric field on the remaining strip metallization (curves $\mathbb{C}_1,\mathbb{C}_2,\mathbb{C}_3,\mathbb{C}_4$) as well as the continuity conditions for the magnetic field on the dielectric–air interface (curve $\mathbb{C}_Q$) are satisfied by using test points on these curves. This results in the following set of homogeneous equations:

$$\overleftrightarrow{M}'\cdot\vec{K}'=\vec{0} \tag{14}$$

where $\vec{K}'$ is given by

$$\vec{K}'=(A_1,\cdots,A_N,B_1,\cdots,B_N)^T. \tag{15}$$

In this case the relationship between the number of boundary points and the truncation index N becomes

$$2\cdot\sum_{\nu=1}^{4}P_\nu+2\cdot Q=2\cdot N. \tag{16}$$

The advantage of method 3 in comparison to methods 1 and 2 is that when choosing the same number of eigenfunctions the rank of the matrix $\overleftrightarrow{M}'$ is halved.

III. Definition of the Characteristic Impedance Z_L

Different definitions of the characteristic impedance of a microstrip line are given in the literature (e.g. [8]). In this paper the definition based on the current and the power transported in the z direction is used. The current I_z is given by

$$I_z=\oint_{\mathbb{C}}\vec{H}\cdot d\vec{s} \tag{17}$$

with

$$\mathbb{C}=\bigcup_{\nu=1}^{5}\mathbb{C}_\nu \tag{18}$$

whereas the transmitted power is described by the Poynting vector:

$$P_z=\frac{1}{2}\cdot\sum_{k=1}^{5}\iint_{\mathbb{A}_k}\vec{E}\times\vec{H}^*\cdot\vec{u}_z\,d\mathbb{A}. \tag{19}$$

The subdivision of the cross section of the shielded microstrip line into subareas $\mathbb{A}_\nu$ is demonstrated in Fig. 3.

It is worth noting that because of the symmetry Fig. 3 shows only one half of the considered microstrip line. Therefore the characteristic impedance of the complete line has to be calculated as follows:

$$Z_L=\frac{P_z}{I_z^2}. \tag{20}$$

IV. Numerical Results

The following numerical results have been calculated with respect to two different geometries at a frequency of $f=30$ GHz. The considered waveguides are characterized by:

microstrip line 1	microstrip line 2
$c=1.2$ mm	$c=6.0$ mm
$d=0.5$ mm	$d=2.5$ mm
$e=1.0$ mm	$e=5.0$ mm
$h=0.635$ mm	$h=0.635$ mm
$\epsilon_r=2.33$	$t=35\ \mu$m
	$\epsilon_r=2.33$.

In case of structure 1 two different metallization thicknesses are used:

$$t_1=10\ \mu\text{m (line 1a)}$$

$$t_2=3.5\ \mu\text{m (line 1b)}.$$

It should be pointed out that in the case of microstrip line 1 the substrate height is nearly half the height of the shielding, which is not usual in the case of microstrip circuits.

Results have been calculated using an equidistant distribution of test points since this has shown the most favorable characteristics for convergence of the solution. When choosing test points on $\mathbb{C}_1$ and $\mathbb{C}_5$, respectively, it should be taken into account that Fig. 2 shows only one half of the total microstrip line. Hence, equidistant distribution of the test points on the metallization is given by

$$x_{P1}(i)=\frac{d-R_1}{2P_1-1}\cdot(2i-1),\qquad i=1\cdots P_1. \tag{21}$$

This guarantees that the distance between $x_{P1}(1)$ and its mirror point on the symmetry plane is exactly the same as the gap between two successive points on $\mathbb{C}_1$. Because of the relationship between thickness and width of the metallization, initially no test points on $\mathbb{C}_2$, $\mathbb{C}_3$, and $\mathbb{C}_4$ will be considered. The chosen distribution of test points

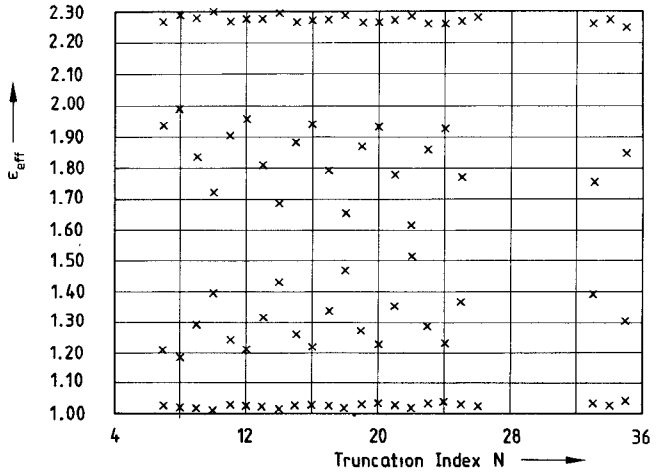

Fig. 4. The dependence of the normalized propagation coefficient $(k_z/k_0)^2 = \epsilon_{eff}$ on the number of eigenfunctions N. Microstrip line 1, $t = 10\ \mu$m, $R_2 = R_1 = 3\ \mu$m, method 1 (boundary conditions on the metallization are satisfied by the potentials).

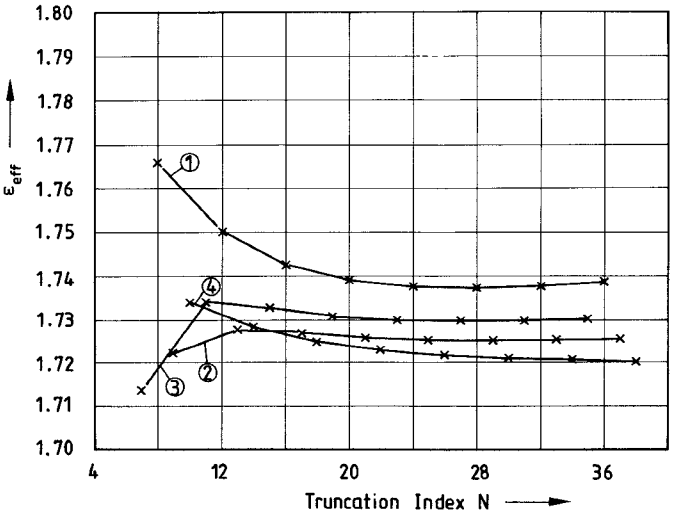

Fig. 5. The dependence of the normalized propagation coefficient $(k_z/k_0)^2 = \epsilon_{eff}$ on the number of eigenfunctions N. Microstrip line 1, $t = 10\ \mu$m, $R_2 = R_1 = 3\ \mu$m, method 2 (boundary conditions on the metallization are satisfied by the tangential components of the electric field).

on the strip boundary is shown in Fig. 3. The consideration of N eigenfunctions leads to

$$P_1 = P_5 = \frac{N}{2} \quad \text{and} \quad Q = N - P_1 \tag{22}$$

if method 1 or method 2 is used.

The calculations of the effective dielectric constant ϵ_{eff} and the impedance Z_L by method 3 require

$$P_1 = \frac{N}{2} \quad \text{and} \quad Q = N - P_1.$$

Figs. 4 through 12 show various numerical results. When the convergence behavior is investigated a special kind of perodicity is observed (Figs. 4–9 and Fig. 12). For all cases apparently four different curves can be recognized. They describe this periodicity of the convergence behavior and are characterized by

- P_1 even and Q even (curve 1)
- P_1 even and Q odd (curve 2)
- P_1 odd and Q even (curve 3)
- P_1 odd and Q odd (curve 4).

Fig. 4 shows the effective dielectric constant as a function of the truncation index N if the microstrip line 1a is analyzed by method 1. In this case the approach fails. Even for large truncation indices (such as $N > 20$) more than one solution for ϵ_{eff} as a function of N can be observed within the interval of $1 < \epsilon_{eff} < \epsilon_r$. It has been observed that some solutions have disappeared at larger truncation indices (for example $N = 26$ and $N = 34$ for the case of P_1 odd and Q odd, shown in Fig. 4). This may cause the misleading conclusion that a satisfactory solution can be obtained. However, this is not the case since convergence cannot be recognized. (It should be pointed out here that truncation indices from $N = 27$ to $N = 32$ have not been analyzed. Therefore, corresponding marks are missing in Fig. 4.)

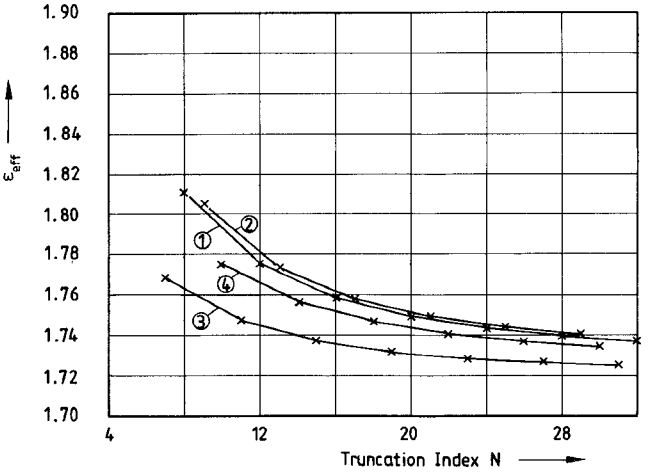

Fig. 6. The dependence of the normalized propagation coefficient $(k_z/k_0)^2 = \epsilon_{eff}$ on the number of eigenfunctions N. Microstrip line 1, $t = 10\ \mu$m, $R_2 = R_1 = 3\ \mu$m, method 3 (combination of PMM and MMT).

Fig. 5 shows the results for the same waveguide if the boundary conditions on the strip metallization are satisfied by the field components instead of the vector potentials (method 2). The corresponding curves which result from the application of method 3 (combination of MMT and PMM) are presented in Fig. 6. However, both of these methods diverge if a thickness larger than 10 μm is chosen for stripline 1. Therefore, numerical results (Fig. 7) are calculated by using method 2 after reducing the strip metallization thickness to 3.5 μm (stripline 1b). For this increased w/t ratio convergence of the effective dielectric constant ϵ_{eff} as a function of the number of considered eigenfunctions N is achieved.

Several numerical calculations of various striplines which are not presented in this paper have shown that best

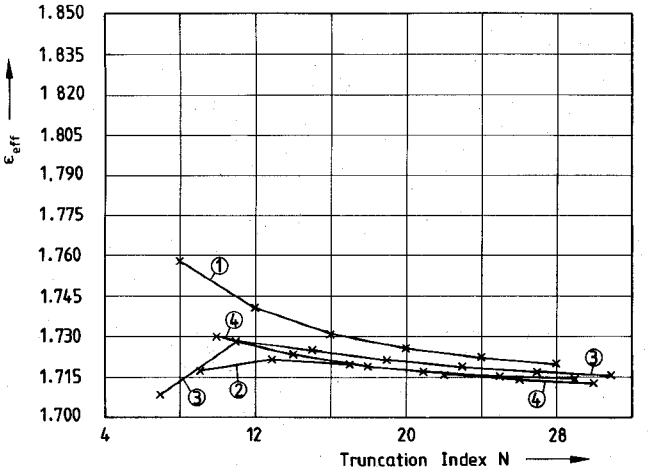

Fig. 7. The dependence of the normalized propagation coefficient $(k_z/k_0)^2 = \epsilon_{eff}$ on the number of eigenfunctions N. Microstrip line 1, $t = 3.5$ μm, $R_2 = R_1 = 0.3$ μm, method 2 (boundary conditions on the metallization are satisfied by the tangential components of the electric field).

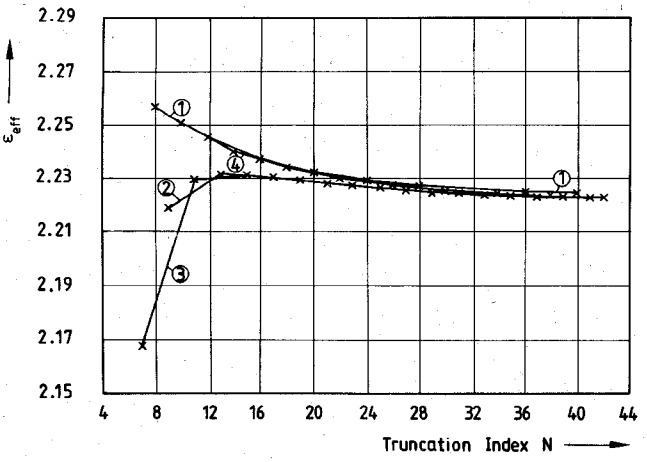

Fig. 8. The dependence of the normalized propagation coefficient $(k_z/k_0)^2 = \epsilon_{eff}$ on the number of eigenfunctions N. Microstrip line 2, $t = 35$ μm, $R_2 = R_1 = 3$ μm, method 2 (boundary conditions on the metallization are satisfied by the tangential components of the electric field).

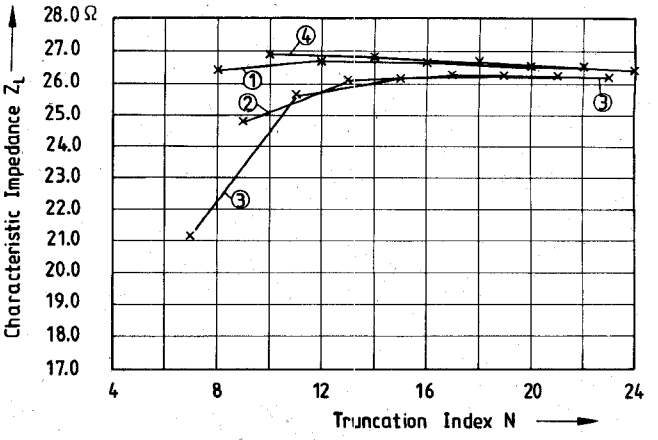

Fig. 9. The dependence of the characteristic impedance Z_L on the number of eigenfunctions N. Microstrip line 2, $t = 35$ μm, $R_2 = R_1 = 3$ μm, method 2 (boundary conditions on the metallization are satisfied by the tangential components of the electric field).

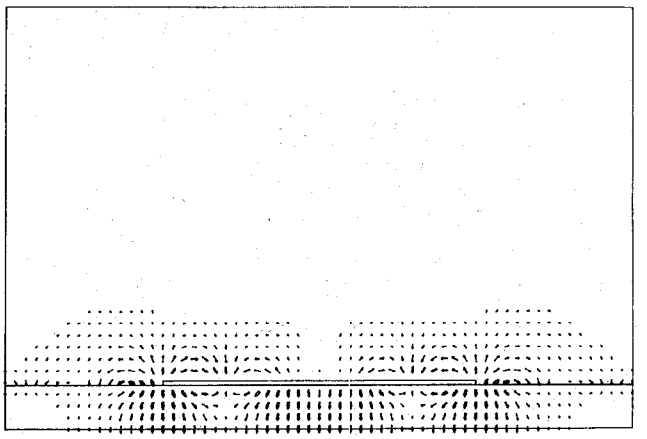

Fig. 10. Distribution of the transverse electric field corresponding to Fig. 8 if $N = 7$ eigenfunctions are taken into account.

results are obtained when the boundary conditions on the strip metallization (at determined test points) have been satisfied by the electric field components. Therefore a further investigation using method 2 will be carried out.

Fig. 8 shows the convergence behavior of ϵ_{eff} if stripline 2 with a metallization thickness of $t = 35$ μm and a shielding height c of nearly ten times the substrate height h is considered by application of method 2 with equidistant test points. It should be pointed out here that a satisfactory convergence for the above metallization thickness will guarantee the convergence for any smaller value as well. Moreover, a good convergence behavior of the effective dielectric constant ϵ_{eff} will justify a sensible calculation of the characteristic impedance Z_L. Because of the good convergence behavior of ϵ_{eff} in Fig. 8, the corresponding characteristic impedance Z_L has been calculated (Fig. 9). Good convergence behavior for Z_L is also observed. However, correct field distribution is only obtained for large truncation indices (for example $N = 38$, Fig. 11) while lower values (for example, $N = 7$) will lead to incorrect field distributions (as shown in Fig. 10) even though ϵ_{eff} and Z_L proved to be convergent.

Several calculations have shown the necessity of considering not only the convergence behavior of ϵ_{eff} and Z_L but also of the field distribution. The following will be given as an example:

The calculation of stripline 1a ($t = 10$ μm) by method 3 using only one test point on $\mathbb{C}_3$ leads to a good convergence behavior for ϵ_{eff} (Fig. 12). Even though the converged value of $\epsilon_{eff} \approx 1.7$ seems to be in accordance with available results (by using MMT), the associated field distribution (shown in Fig. 13, truncation index $N = 21$) is incorrect. The strong concentration of the transverse electric field on the shielding around the dielectric interface cannot be explained physically. The coincidence between the calculated value of ϵ_{eff} and that available in the literature is only a matter of chance.

Hence from the foregoing results the following facts should be pointed out:

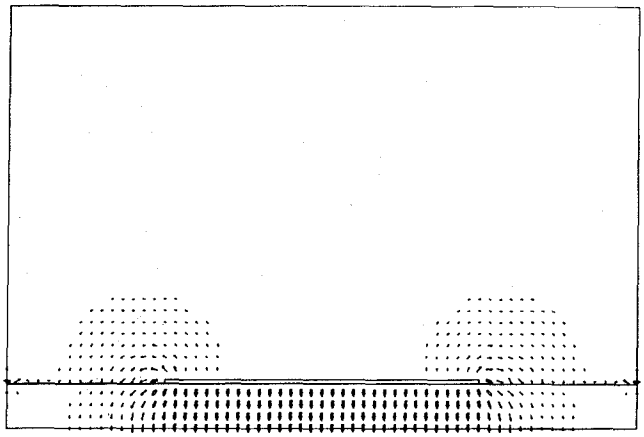

Fig. 11. Distribution of the transverse electric field corresponding to Fig. 8 if $N = 38$ eigenfunctions are taken into account.

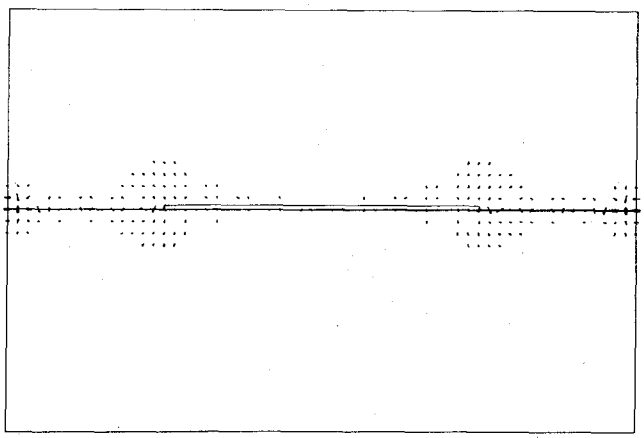

Fig. 13. Distribution of the transverse electric field corresponding to Fig. 12 if $N = 21$ eigenfunctions are taken into account.

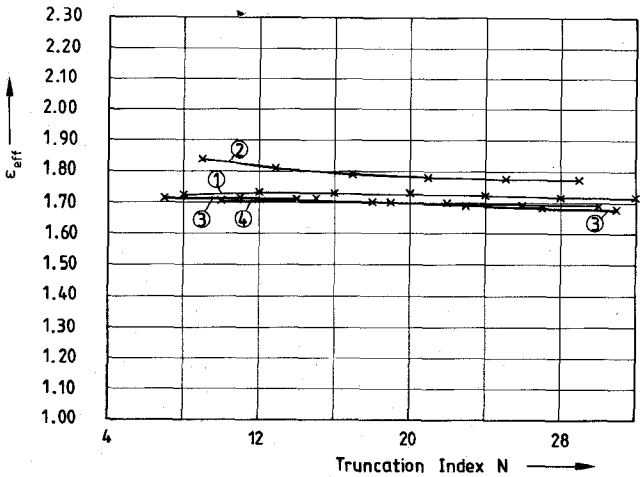

Fig. 12. The dependence of the normalized propagation coefficient $(k_z/k_0)^2 = \epsilon_{eff}$ on the number of eigenfunctions N. Microstrip line 1, $t = 10$ μm, $R_2 = R_1 = 3$ μm, method 3 (combination of PMM and MMT) *with one test point chosen on* $\mathbb{C}_3$ ($P_3 = 1$).

1) Best results are obtained by choosing equidistant test points, i.e., a subdivision of the boundary corresponding to the geometry (see Fig. 3).
2) It is necessary to check the obtained numerical results by validating the correctness of the field distribution.

V. Conclusions

This paper has pointed out the possibilities and difficulties in analyzing the characteristics of shielded microstrip lines with finite strip metallization thickness using the PMM. This approach is based on satisfying the boundary conditions at discrete boundary points, which is quite understandable. However, the examples presented call attention to the necessity of proving the validity of the obtained solutions by other criteria. This is because good convergence behavior of the effective dielectric constant ϵ_{eff} does not always guarantee the correct characteristic impedance or field distribution. In particular, field distribution can be considered as a reliable check for the numerical results.

Another disadvantage of the PMM is the strong correlation between the number of boundary points considered and the rank of the system matrix $\overleftrightarrow{M}$. Since each of the test points is described by different coordinates, the number of equations cannot be reduced analytically. Therefore computation time and storage requirements rise drastically if a sufficient number of eigenfunctions have to be taken into account.

Nevertheless, calculating the transmission properties of microstrip lines with high w/t ratios using the PMM may lead to acceptable results.

References

[1] H.-G. Unger, *Elektromagnetische Theorie für die Hochfrequenztechnik, Teil 1.* Heidelberg: Dr. Alfred Hüthig Verlag, 1981.
[2] R. H. T. Bates, "The theory of the point-matching method for perfectly conducting waveguides and transmission lines," *IEEE Trans. Microwave Theory Tech.*, vol. MTT-17, pp. 294–301, June 1969.
[3] J. A. Fuller and N. F. Audeh, "The point-matching solution of uniform nonsymmetric waveguides," *IEEE Trans. Microwave Theory Tech.*, vol. MTT-17, pp. 114–115, Feb. 1969.
[4] H. Y. Yee and N. F. Audeh, "Uniform waveguides with arbitrary cross-section considered by the point-matching method," *IEEE Trans. Microwave Theory Tech.*, vol. MTT-13, pp. 847–851, Nov. 1965.
[5] R. F. Harrington, "Matrix methods for field problems," *Proc. IEEE*, vol. 55, pp. 136–149, Feb. 1967.
[6] L. Lewin and E. D. Nielsen, "On the inadequacy of discrete mode-matching techniques in some waveguide discontinuity problems," *IEEE Trans. Microwave Theory Tech.*, vol. MTT-18, pp. 364–372, July 1970.
[7] L. Lewin, "On the restricted validity of point-matching techniques," *IEEE Trans. Microwave Theory Tech.*, vol. MTT-18, pp. 1041–1047, Dec. 1970.
[8] R. K. Hoffmann, *Integrierte Mikrowellenschaltungen.* Berlin: Springer Verlag, 1983.

✠

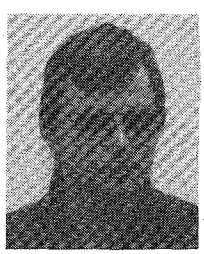

Stefan Kosslowski (M'88) was born in Duisburg, West Germany, on February 6, 1963. He received the Dipl.-Ing. degree in electrical engineering from the University of Duisburg, West Germany, in 1987. He is currently working towards the Dr.-Ing. degree in electrical engineering in the Institute of Electromagnetic Theory and Engineering at the University of Duisburg.

Frank Bögelsack (M'86) was born in Berlin, West Germany, on March 25, 1956. He received the Dipl.-Ing. degree in electrical engineering from the Technical University of Braunschweig, West Germany, in 1983. Since then he has been working in the Institute of Electromagnetic Theory and Engineering at the University of Duisburg, where he is engaged in the numerical computation of electromagnetic fields applied to microstrip discontinuity problems.

Ingo Wolff (M'75–SM'85–F'88) was born in Köslin, Germany, in 1938. He studied electrical engineering at the Technical University of Aachen and received the Dipl.-Ing. degree in 1964. In 1967 he received the doctoral degree and in 1970 the habilitation degree, again from the Technical University of Aachen, West Germany.

From 1970 to 1974 he was a Lecturer and Associate Professor for high-frequency techniques in Aachen. Since 1974 he has been a Full Professor of electromagnetic field theory at the University of Duisburg, Duisburg, West Germany. His main areas of research interests are electromagnetic field theory applied to the CAD of MIC's and MMIC's, millimeter-wave components and circuits, and field theory of anisotropic materials.